

# A Primer on Functional Magnetic Resonance Imaging

Gregory G. Brown · Joanna E. Perthen ·

Thomas T. Liu · Richard B. Buxton

Received: 22 March 2007 / Accepted: 24 March 2007

© Springer Science+Business Media, LLC 2007

**Abstract** In this manuscript, basic principles of functional magnetic resonance imaging (fMRI) are reviewed. In the first section, two intrinsic mechanisms of magnetic resonance image contrast related to the longitudinal and transverse components of relaxing spins and their relaxation rates,  $T_1$  and  $T_2$ , are described. In the second section, the biophysical mechanisms that alter the apparent transverse relaxation time,  $T_2^*$ , in blood oxygenation level dependent (BOLD) studies and the creation of BOLD activation maps are discussed. The physiological complexity of the BOLD signal is emphasized. In the third section, arterial spin labeling (ASL) measures of cerebral blood flow are presented. Arterial spin labeling inverts or saturates the magnetization of flowing spins to measure the rate of delivery of blood to capillaries. In the fourth section, calibrated fMRI, which uses BOLD and ASL to infer alterations of oxygen utilization during behavioral activation, is reviewed. The discussion concludes with challenges confronting studies of individual cases.

**Keywords** Functional magnetic resonance imaging · Perfusion magnetic resonance imaging · Regional blood flow · Cerebral oxygen metabolism

---

G. G. Brown (✉)  
Psychology Service (MC 116B), VA San Diego Healthcare System, 3350 La Jolla Village Drive, La Jolla, California 92161, USA  
e-mail: gbrown@ucsd.edu

G. G. Brown  
Department of Psychiatry, University of California San Diego, San Diego, California, USA

J. E. Perthen · T. T. Liu · R. B. Buxton  
Department of Radiology, University of California San Diego, San Diego, California, USA

Functional magnetic resonance imaging (fMRI) provides a sensitive, noninvasive tool for mapping patterns of activation in the working human brain. However, how this tool works is far from obvious, and to understand the strengths and limitations of fMRI it is necessary to delve into the nature of the magnetic resonance (MR) signal and how it is affected by brain activation. The phenomenon of nuclear magnetic resonance (NMR) is that certain nuclei, when placed in a magnetic field, are able to absorb energy from an electromagnetic field oscillating at a particular frequency (the resonance frequency). In addition, after being excited in this way the nuclei can transfer energy back to a nearby detector coil at the same frequency, like a bell that rings after being struck. Also like a bell, the MR signal slowly fades away, and the time constant for this decay varies in different tissues. An additional key aspect of the NMR phenomenon, which lies at the heart of MR imaging, is that the resonance frequency is precisely proportional to the magnetic field at the location of the nucleus. If a gradient field, a magnetic field that varies in magnitude in a simple linear fashion along a particular spatial axis, is applied to a sample in the magnet, the resonance frequency also varies in a simple linear way along that spatial axis. The returned MR signal is then not a single frequency, but a mix of frequencies, with the amplitude of each frequency corresponding to the signal amplitude arising from a particular location. Taking the Fourier Transform of the measured signal, to break the signal into its component frequencies, produces a map of the amplitude of the MR signal at different locations—an image (Twieg, 1983). The interesting—and unexpected—phenomenon that makes fMRI possible is that the decay time of the MR signal is very slightly lengthened in response to brain activity. However, it is not the neural activity itself that causes this, but rather the changes in local blood oxygenation that accompany neural activation. This blood oxygenation level dependent (BOLD)

effect is the basis for most of the fMRI studies done today, and while it provides a sensitive mapping tool, a quantitative physiological interpretation of the magnitude of the BOLD response is more problematic. Fortunately, other fMRI techniques have been developed that provide additional windows on brain activation, although these methods are not as widely available. In this primer we focus on three MR methods to image brain activity: BOLD contrast, arterial spin labeling (ASL) perfusion imaging, and calibrated-BOLD functional MR imaging. The proper application of MR brain-mapping methods requires an understanding of the biophysical basis of these functional imaging methods. This primer attempts to provide these basic principles. More comprehensive discussions can be found in Buxton (2002), Jezzard, Matthews, and Smith (2001), and Huettel, McCarthy, and Song (2004).

### Selective survey of magnetic resonance principles

In nearly all fMRI studies, the signal being measured arises from hydrogen nuclei, simple protons, which are readily abundant in biological tissue. Although an accurate description of the behavior of individual nuclei in a magnetic field requires an understanding of quantum mechanics, a classical physics view is sufficient to understand the basic behavior of populations of MR observable nuclei given one key concept from quantum mechanics: protons possess an intrinsic property called “spin,” which forms the basis of the NMR phenomenon. Spin is a quantum mechanical property that refers to the intrinsic angular momentum of an elementary particle (Buxton, 2002). Importantly for MR imaging, elementary particles possess intrinsic magnetism that is proportional to their angular momentum (Daniels & Alberty, 1966).

As a rough analogy, we may imagine a hydrogen proton as a magnetic sphere that is rotating about its axis. When placed in an external magnetic field (referred to as the  $B_0$  field), hydrogen protons will tend to align with the external field, in a manner similar to a compass needle aligning with the earth’s magnetic field. Protons aligned with the field are in their lowest energy state, while protons anti-parallel to the external field are in the highest energy state (it takes work to point a compass needle in the direction opposite to the earth’s magnetic field). In a large sample of protons, the tendency of the proton spins to align with the magnetic field is opposed by thermal interactions that tend to equalize the spins aligned with and against the field. For a typical clinical magnetic field strength of 1.5 Tesla (T), the difference between the average number of spins aligned with the field and the average number of spins opposed to the field is only about 1 part in 100,000. Nevertheless, this small difference is enough to create a weak equilibrium magnetization (referred to as  $M_0$ ) that is aligned with the main field. The time constant for alignment with the field, and thus for the crea-

tion of  $M_0$ , is called the longitudinal relaxation time, and is referred to as  $T_1$ . At typical magnetic field strengths used for human brain imaging,  $T_1$  is about one second in gray matter, a little shorter in white matter, and substantially longer (4–5 seconds) in cerebrospinal fluid (CSF).

The source of the resonance of the nuclei is a bit more complicated, and arises when the spin axis is tipped at an angle to the main magnetic field. The interaction of the magnetic moment with the magnetic field tends to make the nuclei align with the field, as described above. But because the protons also have angular momentum, the application of the external field initially leads the protons to precess around the axis of the field, in a manner similar to a gyroscope precessing in the presence of the earth’s gravity field. That is, the spin axis rotates around the axis of the magnetic field. The rate at which the proton precesses is proportional to the magnetic field and is called the Larmor frequency. For a 1.5 Tesla system, the Larmor frequency is 63.85 MHz (millions of cycles per second) for hydrogen nuclei. As noted above, a key method in MR imaging is the use of gradient fields, which produce linear spatial-variations in the magnetic field. The application of gradient fields causes spins at different spatial locations to precess at different frequencies. The spatial heterogeneity of precession frequencies codes location and can be used to form images.

The significance of the resonance frequency is that an additional magnetic field, perpendicular to the main field and oscillating at precisely the resonance frequency, can be used to tip over the equilibrium magnetization of a sample. This creates a precessing magnetization that in turn creates a detectable signal in a nearby detector coil. This additional magnetic field is referred to as the  $B_1$  field, and because it oscillates in the radio frequency (RF) range, and is only on for a short time, it is referred to as an RF pulse. While the  $B_1$  field is turned on, the magnetization follows a widening spiral, gradually tipping away from the main magnetic field  $B_0$  (see Fig. 1A). The net result at the end of the RF pulse is that the magnetization is tipped away from the main magnetic field by an angle called the flip angle (or tip angle). One can think of this as splitting the original equilibrium magnetization into two components: a residual component along the longitudinal axis defined by the main magnetic field  $B_0$  (the  $z$ -axis), and a precessing component at right angles to the main magnetic field, described as lying in the transverse plane ( $x$ – $y$  plane) (see Fig. 1B). Prior to the RF pulse, the transverse components of spins are randomly oriented and so sum to zero, and the effect of the RF pulse is to create a coherent transverse component. Compare the random directions of the spins in Fig. 1C before the  $B_1$  field is applied with the more coherent alignment of the spins after the net magnetization has been tipped (Fig. 1D). The measured MR signal is directly proportional to the magnitude of the coherently precessing transverse magnetization.

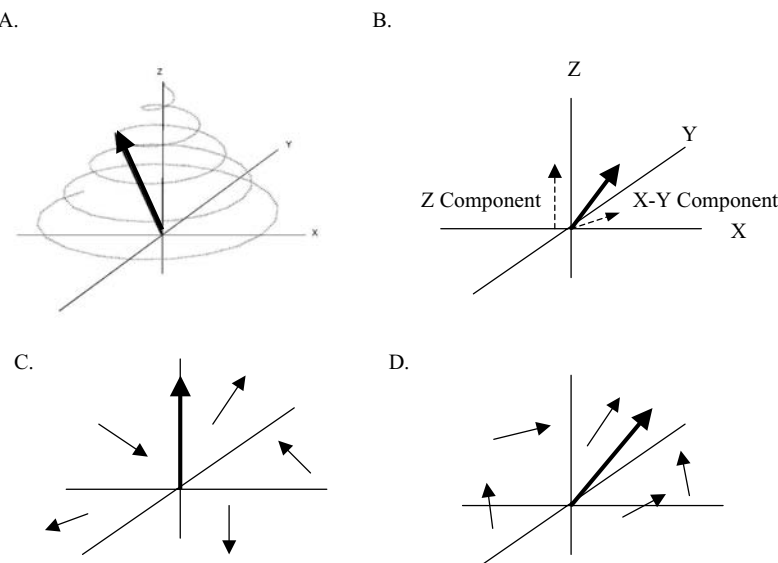


**Fig. 1** Behavior of the net magnetization vector (large arrow) during a magnetic resonance imaging experiment. A. The net magnetization vector precessing in a widening spiral during the delivery of a radio frequency pulse. B. Precessing of the net magnetization vector can be represented by a residual component projected onto the Z-axis and a

precessing component that is projected onto the  $x-y$  plane. C. At rest the orientations of individual precessing spins that compose the net magnetization vector are random. D. During the delivery of the radiofrequency pulse the orientation of the individual precessing spins begin to align or cohere. (Not all spins are shown in Figs. 1C and 1D.)

Because the alignment of the original magnetization with  $B_0$  is the lowest energy state, tipping the magnetization away from  $B_0$  can be viewed as the spin system absorbing energy from the oscillating  $B_1$  field. Although the applied field is very small, typically about 100,000 times smaller than the main  $B_0$  field, it is able to tip the magnetization because it is applied “on resonance” at the precession frequency of the spins. As a useful analogy, imagine using light finger presses to set in motion a large and heavy pendulum. Although each finger press exerts only a light force, the repeated application of finger presses can set the pendulum into motion if the presses are applied at the resonant frequency of the pendulum (Buxton, 2002, p. 73).

The flip angle achieved by the applied RF pulse is controlled by adjusting the amplitude or duration of  $B_1$ . For a 90-degree flip angle, the magnetization is tipped completely into the transverse plane, with no residual longitudinal magnetization. For a 180-degree flip angle, the magnetization is tipped into a direction that is directly opposite to the equilibrium orientation. An RF pulse that results in a 180-degree flip angle is referred to as an **inversion** pulse, because it inverts the direction of the magnetization. Note that an inversion pulse by itself does not create any measurable MR signal, because there is no transverse magnetization, but it does serve to mark the magnetization at a particular time. As discussed below, inversion pulses are widely used in arterial spin labeling to invert the magnetization and effectively tag arterial spins before they flow into the imaging region.

Once the radiofrequency field has been turned off, the population of hydrogen protons will gradually return to its

equilibrium or lowest energy state. The longitudinal component of magnetization (e.g., along the direction of the main field) will return in an exponential fashion to its equilibrium value  $M_0$  with the longitudinal relaxation time constant  $T_1$ . For example, after the application of an inversion pulse, the magnetization will relax from its initial value of  $-M_0$  to its equilibrium value of  $M_0$ . For arterial blood,  $T_1$  is about 1300 ms at 1.5 Tesla, so that the longitudinal magnetization is fully relaxed after about 5 time constants (6.5 seconds). The transverse component of magnetization decays exponentially with the transverse relaxation time constant  $T_2$ . Transverse relaxation reflects the random interaction of spins in a manner that causes neighboring spins to precess slightly out of phase. For fully oxygenated arterial blood at 1.5 Tesla,  $T_2$  is about 240 ms, so that the transverse magnetization will completely decay after about 1.2 seconds. Transverse relaxation can also occur due to the dephasing caused by the presence of local field inhomogeneities that cause spins at different locations to precess at different frequencies. The transverse relaxation due to all sources, including those due to spin-spin dephasing ( $T_2$ ), is characterized by the apparent transverse relaxation time constant  $T_2^*$ , which is typically on the order of 50 milliseconds in gray matter.

A somewhat confusing feature of this picture of NMR is that  $T_1$  is typically nearly an order of magnitude longer than  $T_2$ . Because of this, we cannot think of the relaxation back towards equilibrium as a vector slowly flipping back up, the reverse of the process of tipping over the magnetization with the RF pulse. Rather, we need to think of it as two processes in parallel acting to restore the equilibrium state in which

there is a longitudinal magnetization  $M_0$  but no transverse magnetization. To that end, the transverse magnetization decays more quickly with a time constant  $T_2$  (or  $T_2^*$ ), while the difference between  $M_0$  and the current longitudinal magnetization ( $M_0 - M_z$ ) decays away more slowly with a time constant  $T_1$ . A critical aspect of MRI is that the local tissue properties  $T_1$  and  $T_2$  interact with the timing of the pulse sequence to affect the magnitude of the resulting MR signal. For example, if another RF pulse is applied before the longitudinal magnetization has fully relaxed, the transverse component—and thus the MR signal—will be reduced because the starting longitudinal magnetization was weaker. In this way the time between RF pulses, called the repetition time TR interacts with  $T_1$  to affect the MR signal. After the RF pulse creates a precessing transverse magnetization, the signal is measured in a short window centered on a time TE (for echo time) after the RF pulse. During the interval, TE, the signal decays with a time constant  $T_2^*$ , so this brings in a sensitivity to the local value of  $T_2^*$  through the choice of TE.

As noted above, the signals from different locations are distinguished by applying field gradients to spread the signals into different frequencies, with frequency corresponding to location. A basic imaging experiment uses a 90-degree pulse to create a precessing transverse magnetization. At time TE after the RF pulse, the signal is measured in the presence of field gradients, and the data are reconstructed into an image. One can think of an MR image as a snapshot of the magnitude of the local transverse magnetization at a time TE after the RF pulse. If the TE is made relatively long (30–50 milliseconds), then the signal magnitude will have a significant sensitivity to the local value of  $T_2^*$  (described as a  $T_2^*$ -weighted signal). The remarkable phenomenon that underlies BOLD-fMRI is that local  $T_2^*$  becomes slightly longer with brain activation, and so appears as a slight increase of the local MR signal.

### Blood oxygen level dependent contrast

#### Biophysical principles

The core MR experiment assumes that the lines of the static magnetic field remain the same throughout the imaging space. Yet variation in the molecular structure of biological substances can concentrate or expand the local lines of the magnetic field, a magnetic susceptibility effect (Elser & Burdette, 2001, p. 133). When magnetic susceptibility varies over a small region, proximal spins will experience different local magnetic fields depending on their location, and will begin to grow out of phase as they precess, reducing the net MR signal. A prominent example of this signal loss occurs in the orbitofrontal cortex when images sensitive to  $T_2^*$  are collected (Fig. 2). This artifact is due to the different magnetic susceptibilities of air in the nasal sinuses, bone, and brain, all being in proximity and producing a complex distortion of the

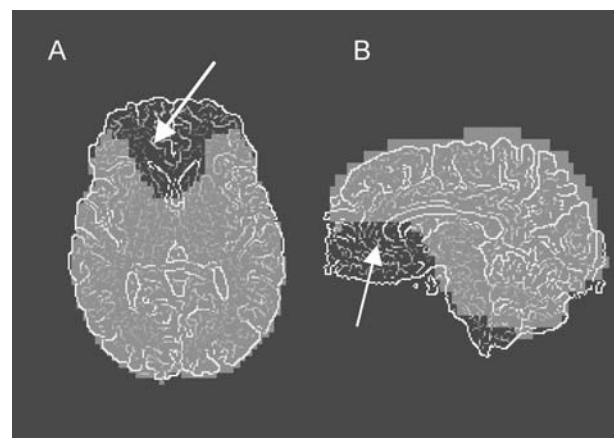


**Fig. 2** A  $T_2^*$ -weighted gradient echo image (light gray image) overlaid onto a high resolution  $T_1$ -weighted image (dark image in white outline). Arrows point to areas of diminished  $T_2^*$ -weighted signal

magnetic field lines (Buxton, 2002). As frequently happens in MR research, one scientist's artifact is another scientist's science. Although susceptibility effects can produce artifacts when imaging anatomy, they are central to the generation of the blood oxygen-level dependent (BOLD) contrast that is the basis of most functional MRI studies.

The magnetic susceptibility effect at the basis of BOLD experiments arises from the biophysics of the hemoglobin molecule, which provides oxygen required for aerobic energy metabolism (Gjedde, 2001). As blood leaves the lungs, oxygen becomes loosely and reversibly bonded to an iron atom that lies at the center of the heme molecule within the hemoglobin complex (Guyton, 1977, pp. 58–59). When delivered to tissue, oxygen separates from the heme molecule exposing electrons from the iron atom. The unpaired iron electrons alter the lines of the magnetic field near the deoxyhemoglobin molecule. This susceptibility effect causes slight dephasing of the spins of the hydrogen nuclei in proximal water molecules. The dephasing of spins occurs both inside blood vessels and in adjacent tissue (Buxton, 2002).

The intravascular susceptibility can be understood by considering a mixture of hemoglobin and deoxyhemoglobin molecules inside a cylinder. This simple model predicts that the magnitude of the intravascular susceptibility effect is related to the relative concentrations of oxygenated and deoxygenated hemoglobin. Thulborn and colleagues (1982) confirmed this prediction when they found that the apparent transverse relaxation time of water protons in whole blood linearly varied with blood oxygenation. Because blood vessels represent only about four percent of the total brain volume, it might be expected that intravascular susceptibility effects would be small. Yet at a field strength of 1.5 Tesla, about half of the BOLD contrast is due to the intravascular signal (Boxerman et al., 1995a).

The extravascular susceptibility effect can be understood by treating the blood vessel as a long cylinder with

homogeneous susceptibility, corresponding to the mean susceptibility averaged over the local oxygenated and deoxygenated hemoglobin. The model assumes that the cylinder is surrounded by a medium with a different magnetic susceptibility. If the cylinder is perpendicular to the static magnetic field, the amount of spin dephasing is determined only by the difference between the internal and external susceptibilities at the surface of the cylinder (Buxton, 2002). Moreover, the radius of the cylinder determines the spatial extent of the dephasing (Buxton, 2002). The effects of deoxyhemoglobin on the magnetic field in adjacent extravascular tissue is larger in tissue adjacent to larger blood vessels, such as veins.

Diffusion, the random movement of water molecules due to thermal perturbations, is a second factor that affects the amount of dephasing of spins forming the extravascular signal. Without diffusion, the phase dispersion between spins at different locations would simply reflect the distribution of magnetic fields caused by the blood vessels containing deoxyhemoglobin. However, with diffusion, as a water molecule moves randomly through these spatially varying fields, the molecule's hydrogen nuclei effectively sample a range of different fields. For this reason, the net phase dispersion between different spins is reduced, and so the same set of field offsets produce less of a change in  $T_2^*$ . The result is that  $T_2^*$  effects are not as pronounced around capillaries, which are small enough for diffusion to be important, compared to veins, where diffusion is less important (Ogawa et al., 1993; Boxerman et al., 1995b). Thus the largest BOLD change in  $T_2^*$ -weighted signals is near veins draining the activated area.

Given that aerobic metabolism increases with neuronal activation, it would be reasonable to infer from the theory described above that increased neuronal activity would cause a decrease in MRI signals sensitive to  $T_2^*$ —because of an increased extraction of  $O_2$  and, thus, an increase of deoxyhemoglobin. Therefore, it was a surprise when early brain activation studies showed increased BOLD signal during behaviorally active conditions (Bandettini et al., 1992; Ogawa et al., 1990). The enhanced BOLD signal is due to an increased delivery of oxygenated blood out of proportion to the utilization of oxygen by neural cells (Buxton, 2002). One current theory is that the exuberant delivery of oxygenated blood is required to keep the oxygen tension of blood high enough to drive oxygen from capillaries to brain cells (Gjedde, 2001). Whatever the precise mechanism, neural activation causes an enhanced delivery of oxygenated blood that makes  $T_2^*$ -weighted MR images brighter.

### Mapping brain activation

Using deoxyhemoglobin as an endogenous tracer, regional brain activation can be mapped with  $T_2^*$  sensitive pulse sequences, such as the gradient recalled echo (GRE) sequence.

Because the mapping is driven by regional changes in the blood level of oxygenated hemoglobin, the most common MR method of measuring brain activation is based on BOLD contrast. Although the term BOLD focuses on oxygenated hemoglobin, the method is best understood as a deoxyhemoglobin washout technique.

From the discussion above, it should be clear that BOLD signals only indirectly reflect neural activity. Figure 3 shows a flow chart of the presumed sequence of events. A stimulus change causes a change in neural activity that, in turn, produces a hemodynamic response, altering cerebral blood flow and cerebral blood volume, and possibly producing a small change in oxygen metabolism. The combined hemodynamic and metabolic changes alter the susceptibility difference between the intravascular red cells and the extravascular brain tissue, dephasing spins within the vessel and in brain tissue. Three important aspects of BOLD contrast should be considered. First, the functional contrast is relative. BOLD contrast always represents a comparison of  $T_2^*$  sensitive signals across two or more behavioral states. Second, BOLD contrast does not reflect a single physiological process, but rather represents the combined effects of blood flow, blood volume, and oxygen utilization. Third, the sluggish response of the vascular system to neural events delays, disperses, and smooths over time the underlying neural signal. The first two points imply that BOLD contrast is not expressible in absolute physiological units. The third point implies that the observed BOLD signal is generally a composite of signals produced by separate neural events. Decomposing this composite signal is facilitated by an understanding of the shape of the BOLD signal arising from a single stimulus. The MR signal plots in Fig. 3 show an idealization of the BOLD signal due to brief stimulation. This signal is complex, with an initial drop followed by the rise to a single maximum, a decline, and an undershoot before returning to baseline (Uludağ et al., 2006). A detailed biophysical explanation of the complex shape of the BOLD signal is a current area of research (Uludağ et al., 2006).

### Experimental design

The composite nature of the BOLD signal must be considered when developing research designs for fMRI studies (Donaldson & Buckner, 2001). One approach is to take advantage of the summed signal as a method of reducing noise in the experiment. Assuming independence of the noise components, a composite MR signal summed over trials will tend to cancel the effects of randomly occurring sources of noise, as in many instances of averaging. Presenting the same class of stimuli in blocks capitalizes on this averaging strategy. Ideally designs involving a block of the same stimuli would yield an MR signal that would rise to a steady plateau and decline once the block ends. Designing efficient block

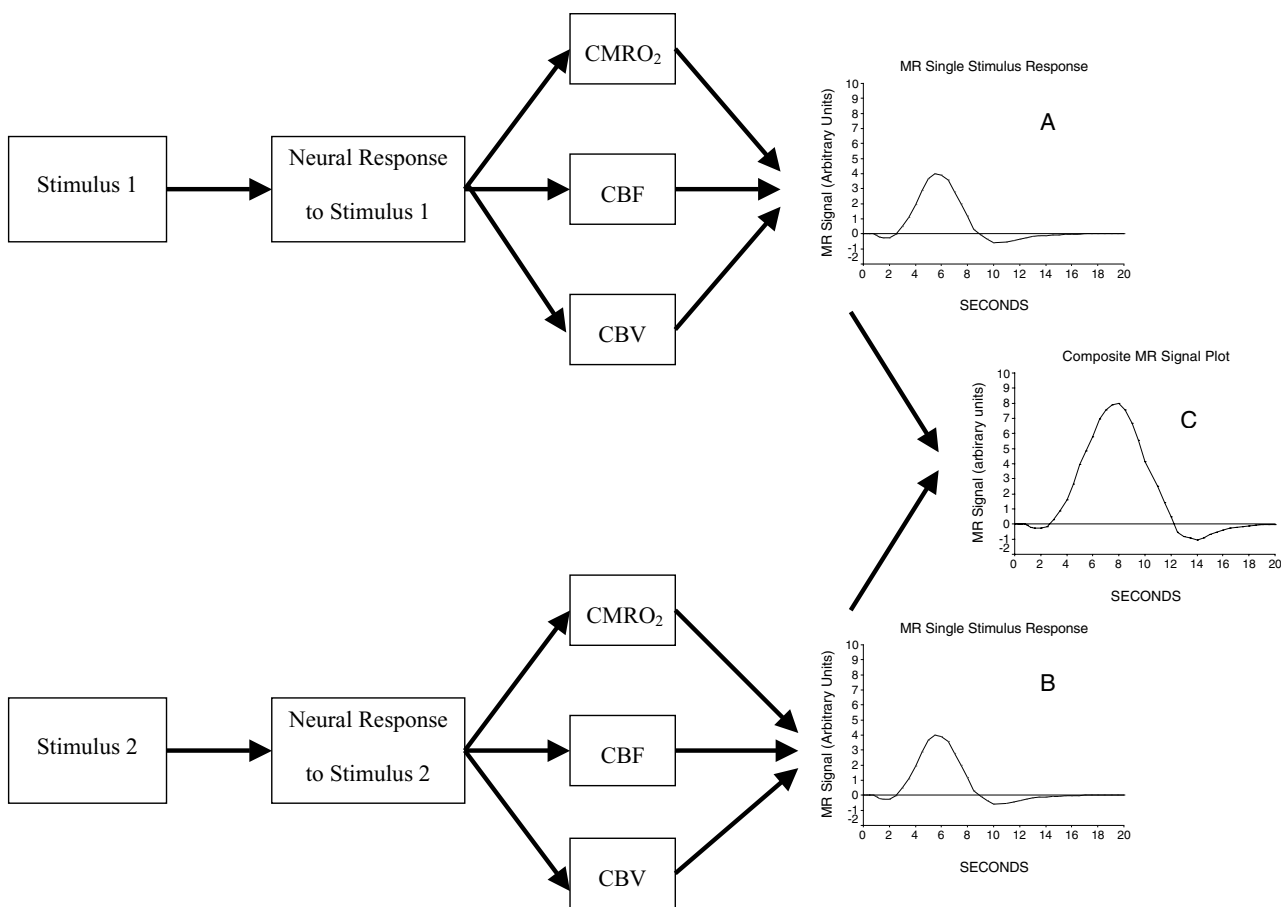


**Fig. 3** Events leading from the presentation of two stimuli to the generation of a summed BOLD signal. The figure assumes that stimulus 1 is presented one second before stimulus 2. Each stimulus elicits a neuronal response that alters the cerebral metabolic rate of oxygen utilization (CMRO<sub>2</sub>), cerebral blood flow (CBF), and cerebral blood

volume (CBV). The net effect of CMRO<sub>2</sub>, CBF, and CBV changes leads to the BOLD response for individual stimuli (A and B). The observed BOLD response (C) is a composite of the unobserved BOLD responses to the single stimuli

designs involves deciding on the number and timing of stimuli to present within a block, the duration of the block, the number of times a specific block type should be repeated, and the number of different classes of stimuli to include during a single run.

A second approach to managing the composite nature of the observed MR signal is to decompose the complex signal into its components. This approach is well suited to single trial or event-related designs. One method of decomposition is to assume a canonical shape to the hemodynamic response to each stimulus and to model the MR signal as the weighted sum of the canonical response to consecutive stimuli (Bandettini & Cox, 2000). The canonical shape method assumes that a consensus about the shape of the hemodynamic response can be reached, and that the impact of consecutive stimuli can be statistically modeled as a linear sum. The first assumption might not be valid even among healthy volunteers and is probably not safe when comparing patients and healthy volunteers (Aguirre et al., 1998). The linearity assumption might not be strictly valid, especially for the

early phase of the hemodynamic responses (Boynton et al., 1996; Friston et al., 1998). Such concerns have led to a second decomposition approach where the mathematical technique of deconvolution is used to infer the underlying hemodynamic response from the observed MR signal produced by a particular string of stimulus or response events (Dale & Buckner, 1997). Each event is assumed to elicit an impulse response that is distributed over time (Dale, 1999). Deconvolution is used to estimate the unknown impulse response function triggered by a series of these events (Dale, 1999). Although the standard deconvolution approach makes a linearity assumption, it does not assume a canonical shape to the data (Karu, 1995). Thus, the deconvolution method can be used to compare groups on differences in the shape of the BOLD response as well as to compare signal magnitude. As with block designs, a sophisticated literature exists on the efficient design of event related or single trial designs (Burock et al., 1998; Dale, 1999; Donalson & Buckner, 2001; Liu et al., 2001; Liu & Frank, 2004; Liu, 2004). Commonly used image analysis packages often provide tools

to study the efficiency of an event related design prior to collecting data.

Block designs typically have more power than event related designs when detecting the magnitude of the BOLD response (Liu et al., 2001). Event-related designs are more efficient at estimating the shape of the hemodynamic response (Liu et al., 2001). Although less powerful in detecting response magnitude, event-related designs can be used to randomize the presentation of stimuli from different stimulus classes (Burock et al., 1998). Event-related designs also allow investigators to examine the BOLD response based on response types, such as comparing correct with incorrect responses or fast versus slow responses. The number of modes in the deconvolved hemodynamic curve can provide information about the timing of latent cognitive processes underlying the observed response (Zarahn et al., 1997). As with all experimental design, the choice between blocked or event-related fMRI designs starts with the study hypotheses.

It is tempting to wish to infer from fMRI data a functional brain substrate that is necessary and sufficient to support the computation of a specific cognitive process. There are at least two constraints on this wish. First, fMRI studies of intact brain cannot validate the necessary involvement of a brain region in the performance of a particular cognitive process. Animal studies of classical conditioning have shown some neurons become activated by the conditioned stimulus even though damage to these neurons does not alter conditioning (Berger, 1984). Thus, the activation of a neuronal pool by a task does not imply that the activated neurons are necessary for successful performance of the task. Second, it is difficult to isolate a specific stage of cognitive processing when using the simple subtraction paradigms commonly used in fMRI studies. Consider a two-condition design where neutral faces are compared with emotional faces. It is tempting to subtract the mean fMRI signal associated with neutral faces from the mean fMRI signal related to the emotional faces in order to isolate the brain processes related to emotion. This logic involves a dual subtraction; one involving cognitive processes, and the other involving MR signals. The logic of cognitive subtraction and its pitfalls were carefully analyzed by Sternberg (1966) decades ago and have been amplified by psychologists since (Townsend & Ashby, 1983). A fundamental problem is with the assumption of pure insertion, which asserts that a cognitive process can be inserted into a series of cognitive stages without altering the function of any process involved (Friston et al., 1996; Sternberg, 1969). The assumption is part of the argument that the effects of various cognitive processes do not interact but, rather, are additive. Simple subtractive designs cannot test for such interactions; factorial designs are required. Parametric designs also provide an alternative to simple subtractive designs. Parametric designs assume that levels of activation of a subprocess can

be experimentally varied without influencing other cognitive processes. If a stimulus can be manipulated without introducing a new cognitive process into the task, the assumption of pure insertion can be avoided. When properly used, parametric designs not only avoid the pure insertion assumption, they are useful in comparing the brain response of patients and healthy volunteers across similar and dissimilar levels of performance and provide useful profile information about brain response to variations of cognitive load.

#### Statistical analysis

The analysis of fMRI signals from blocked designs begins with the behavioral notion of stimulus control. Each change in stimulus type should change the MR signal response. Figure 4 shows this principle for a run where viewing of 30 second blocks of a complex visual stimulus was alternated with viewing of 30 second blocks of a simple orientation cross. The figure presents time-series data from a volume element (voxel) in the ventral occipitotemporal area. Each time the stimuli are switched from the orientation cross to the complex figure, the MR signal increases. Magnetic resonance signals in most other brain regions did not show this tight stimulus control. The coupling of variations in MR signal response to variations of stimulus presentation can be quantified by a regression model where dummy coding of the stimulus condition is used as an independent variable to

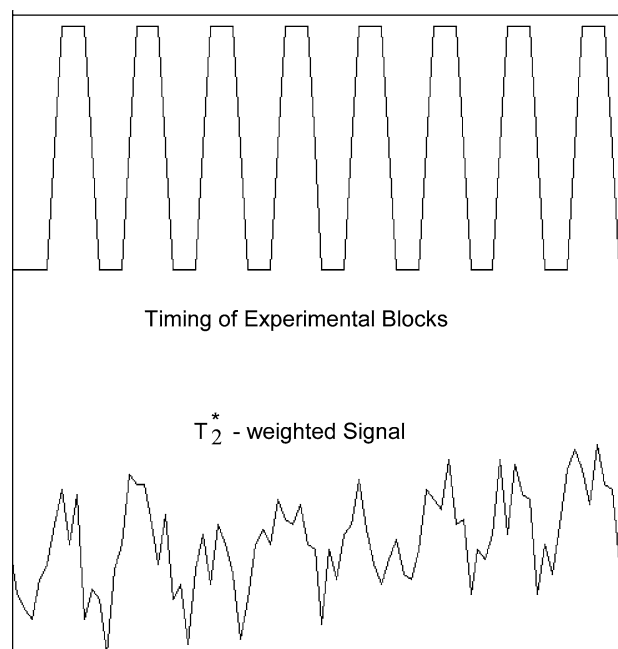


**Fig. 4** Stimulus control of the magnetic resonance signal. The top line shows the timing of alternating blocks of stimuli. The tops of the trapezoids show when complex visual figures were presented. The bottoms of the trapezoid show when the orientation cross was presented. The sides are sloped to model the rise and relaxation times of the hemodynamic response. The bottom line shows the  $T_2^*$ -weighted signal

predict the MR signal response. The correlation coefficient from this analysis can be used to measure the consistency of the stimulus control, whereas the regression weight can be used to measure the magnitude of the BOLD response. The correlation coefficient is usually improved if a shift term is included in the analysis (Cohen, 1997). The regression analysis is typically performed for each voxel with the resulting regression weights presented as a brain map. These weights are the primary dependent variables in group-analyses and can be analyzed with standard parametric or non-parametric statistics.

For event related designs involving a canonical hemodynamic model, a regression weight is estimated to convey the contribution of the canonical hemodynamic response to signal variability within a voxel across all time points (Bandettini & Cox, 2000). This weight can be used as a dependent variable in group-analyses. When the shape of the hemodynamic response is estimated, some feature of the shape, such as its area or the value at its highest peak can be used as a dependent variable in group-analyses. Regression models for both blocked and event related designs may include nuisance covariates, such as measures reflecting subject movement, when estimating the magnitude of the BOLD response.

### Perfusion functional MR imaging

Arterial spin labeling is the primary MRI method used to measure cerebral perfusion. Arterial spin labeling magnetically labels the water molecules of flowing blood to produce an endogenous blood flow tracer (Liu & Brown, 2007). The magnetic label is typically introduced by saturating (i.e., nulling) or inverting the longitudinal ( $z$ -axis) component of the MR signal (Fig. 1a). Whereas BOLD contrast depends on  $T_2^*$  mechanisms, ASL perfusion depends on  $T_1$  effects.

The tagged water passes from the capillaries into brain tissue, where it alters the local tissue's longitudinal magnetization (Aguirre et al., 2005). The greater the flow into the imaging slice, the greater the signal changes in the tagged condition compared with an untagged control condition. Most ASL methods measure CBF by taking the difference between *tag images*, in which the longitudinal magnetization of arterial blood is inverted or saturated, and *control images*, in which the magnetization of arterial blood is fully relaxed. The raw tagged image contains a large contribution of static magnetization that can obscure the signal change related to perfusion. If carefully acquired, the *control image* contains the same static magnetization as the tagged image but not the blood flow effects produced by the magnetic tracer. Thus, the difference between the control and tag images yields an image  $\Delta M = M_{\text{control}} - M_{\text{tag}}$  that is proportional to CBF. Tag and control images are typically acquired in a temporally

interleaved fashion, with a variety of difference methods available to calculate changes in blood flow (see below). In a typical ASL experiment, about one second is allowed for the delivery of blood, corresponding to one ml of blood delivered to 100 ml of tissue. As a result, the overall MR signal due to the delivered blood is only about 1% of the total signal due to the tissue. This small percentage contributes to the low intrinsic signal-to-noise ratio (SNR) of ASL methods.

### Arterial spin labeling methods

Three classes of ASL methods are currently available. Variation in these methods depend on how the magnetic labeling process tags the location and velocity of flowing blood.

*Pulsed Arterial Spin Labeling—tagging based on location.* Pulsed arterial spin labeling (PASL) uses short (5–20 millisecond) radiofrequency pulses to saturate or invert a slab of static and flowing spins in the **tagging region**, proximal to the **imaging slice** (Edelman et al., 1994). *Pulsed arterial spin labeling* has a high inversion efficiency and uses little radiofrequency power. There exists a variety of PASL methods, such as EPISTAR (Edelman et al., 1994), FAIR (Kim & Tsakos, 1997; Kwong et al., 1995), and PICORE (Wong et al., 1997). Although the implementation details of the tag and control conditions differ across these methods, they all tend to give very similar perfusion results (Wong et al., 1997).

*Continuous Arterial Spin Labeling—tagging based on location and velocity.* Continuous arterial spin labeling (CASL) uses long (1–3 second) radiofrequency pulses in conjunction with a constant gradient field to irradiate a narrow plane of spins with radiofrequency energy (Alsop, 2005). The irradiated plane is chosen so that arterial blood flows through the irradiated plane in a direction that is roughly perpendicular to the plane. By properly adjusting the amplitude of the RF and gradient fields, inflowing spins within a physiological range of velocities will be labeled based on a phenomenon termed flow-driven adiabatic inversion (Detre et al., 1992). Because the CASL tag can be applied closer than PASL to the imaging region (on average), the continuous ASL can result in a higher overall tagging efficiency than PASL. Continuous arterial spin labeling requires a large amount of average radiofrequency power that can approach system performance limits and FDA guidelines (Alsop, 2005). System performance limitations have been addressed for the most part by a recently introduced form of CASL, dubbed pseudo-CASL, which uses repeated radiofrequency pulses instead of a continuous radiofrequency signal (Garcia et al., 2005). Wong and colleagues provide a detailed comparison of pulsed and continuous ASL techniques (Wong et al., 1998b).

*Velocity Selective Arterial Spin Labelling—tagging based on velocity.* The velocity selective arterial spin labelling

(VS-ASL) tagging method selectively saturates flowing spins with no spatial selectivity (Wong et al., 2006). This velocity selective saturation is accomplished with a radiofrequency and gradient pulse train that effectively dephases the MR signal from protons flowing faster than a specified cut-off velocity while rephasing the signal from slower flowing protons. At a threshold velocity of one cm/sec, the sequence dephases spins in arterioles that are approximately 50 microns or more in diameter. In principle, VS-ASL results in a small and uniform transit delay for the delivery of the tagged blood to the tissues of interest.

### Data processing

In most ASL-fMRI experiments, control and tag images are acquired in an interleaved fashion. A perfusion time series is then formed from the running subtraction of the control and tag images. In a scheme called surround subtraction, the perfusion images are formed from the difference between each control image and the average of the two surrounding tag images or from the difference between the average of two surrounding control images and a tag image. Other common approaches are *pairwise subtraction* and *sinc subtraction*. In pairwise subtraction consecutive pairs of images are subtracted. In sinc subtraction the images are weighted by a sinc function before subtraction. A general analytic model can be used to compare these three methods of subtraction (Liu & Wong, 2005). For block designs studies (e.g., long periods of on/off), surround and sinc subtraction perform well (Aguirre et al., 2002). For randomized event-related designs, pair-wise subtraction can provide better performance (e.g., less filtering of the hemodynamic response function) (Liu & Wong, 2005). Nonetheless, all filtered subtraction approaches broaden the hemodynamic response function. Unfiltered approaches based upon general linear models of the ASL experiment can eliminate this broadening (Liu et al., 2002), and lead to improvements in statistical power (Mumford et al., 2006).

Cardiac and respiratory fluctuations are a major source of noise in ASL experiments, especially at higher field strengths. Because the inherent signal to noise ratio of ASL measurements is typically below that of BOLD-fMRI, methods to reduce physiological noise are especially needed. Image based correction methods using physiological measurements obtained simultaneously with the images can significantly reduce physiological noise in ASL data (Restom et al., 2006).

### *Comparison of ASL and BOLD Activation Measures*

Like BOLD contrast, ASL perfusion can be used to map brain activation. As brain activation mapping techniques, BOLD and ASL have unique strengths and weaknesses. The signal

to noise ratio of the BOLD response is generally greater than the ASL signal (Wong et al., 2000). The temporal resolution of BOLD acquisitions is greater than ASL acquisitions because two images need to be acquired for the ASL method and because a delay interval is needed to wait for blood to flow into the imaging regions. The maximum number of slices is usually greater in BOLD studies than ASL studies (Liu & Brown, 2007). Blood oxygenation level dependent contrast appears to be more sensitive to parametric manipulations of task demands than ASL perfusion (Rao et al., 2000).

Unlike BOLD methods, ASL techniques measure a well-defined physiological quantity, local blood flow. The effects of a disease on baseline perfusion can be studied with ASL in addition to investigating the disease's effect on brain activation. The differencing methods that generate perfusion images minimize the effects of low frequency drifts and make ASL especially useful for experiments with long stimulus durations (Aguirre et al., 2005). The relative stability of ASL perfusion over long durations makes ASL a useful technique to study naturalistic behavioral changes or to study interventions. Arterial spin labeling perfusion measures are localized to the capillary beds and thus may provide better localization information than BOLD contrast. With the use of background suppression methods and spin-echo readouts, ASL functional measures have been shown to be less prone than BOLD to false activations during overt speech paradigms, reflecting the reduced sensitivity to susceptibility artifacts caused by the air volume dynamics involved in speaking (Kemeny et al., 2005).

Unless corrected for physiological confounds, ASL signals fluctuate over time reducing their sensitivity to behavioral manipulations (Restom et al., 2006). Arterial spin labeling maps of brain activation also tend to exhibit smaller activation regions than BOLD maps (Mildner et al., 2005; Tjandra et al., 2005). The smaller spatial extent of the ASL maps might be due to their decreased sensitivity to small activation changes or to their improved signal localization (Liu & Brown, 2007). Some investigators have found that the increased within-subject sensitivity of BOLD measures of brain activation compared with ASL measures is offset by the greater between-subject variation of BOLD (Wang et al., 2003).

As ASL becomes more widely available on commercial scanners, it is likely to increasingly compete with BOLD contrast as a method of fMRI. Each method has strengths that would make it more appropriate to test a particular hypothesis. However a third option, calibrated fMRI, is being developed that integrates information from BOLD contrast and ASL perfusion. The integration permits measurements to be made of differences in the cerebral metabolic rate of oxygen utilization for different behavioral conditions.

## Quantitative functional magnetic resonance imaging

### A probe of brain physiology

Functional MRI methods based on the BOLD effect are in widespread use as a mapping tool for measuring patterns of brain activation in response to a variety of tasks. If a particular brain region shows a sufficiently strong correlation of the BOLD signal with some aspect of the task, it is interpreted as evidence that there is a local change in neural activity associated with that task. However, a quantitative interpretation of the magnitude of the BOLD response as a reflection of the magnitude of the underlying change in neural activity or metabolism is more problematic. The difficulty arises because functional MRI methods are sensitive to the balance of the changes in cerebral blood flow (CBF), cerebral blood volume (CBV) and the cerebral metabolic rate of oxygen metabolism ( $\text{CMRO}_2$ ) that accompany neural activity, rather than the neural activity itself. That is, each of each of these physiological quantities affects the local deoxyhemoglobin content of the blood and so affects the BOLD response, but the coupling of these physiological changes in response to neural activation is still poorly understood. The primary physiological phenomenon that leads to the BOLD effect is that CBF increases much more than  $\text{CMRO}_2$  with activation, but it is unknown whether the degree of mismatch varies with brain region, stimulus type, development, or disease. In short, the BOLD response is very useful for answering the question: where is there activation? But it is much more difficult to use the BOLD response to answer the question: what is the magnitude of the activation?

There are two physiological reasons why the magnitude of the BOLD effect could be dissociated from the magnitude of the underlying physiological changes, both related to the dependence of the BOLD effect on local deoxyhemoglobin. The first is that there is a ceiling on the BOLD effect magnitude set by the amount of deoxyhemoglobin present in the baseline state, and this baseline condition could vary across the brain due to differences in CBV or baseline oxygen extraction fraction (Brown et al., 2003; Miller et al., 2001). In addition, medications or physiological factors could increase baseline CBF without increasing baseline  $\text{CMRO}_2$ , with the result that the baseline oxygen extraction fraction, and the baseline deoxyhemoglobin, would be reduced (Brown et al., 2003). In anticipation of the model described below, we can describe this effect of baseline deoxyhemoglobin by a parameter  $M$  that acts as a multiplicative scaling factor on the BOLD effect. That is, if we compare two regions of the brain with different baseline blood volume fractions, the area with the higher blood volume would have a higher local value of  $M$ , and for the same underlying change in CBF and  $\text{CMRO}_2$  would exhibit a larger BOLD response.

The second potential source of variability in the magnitude of the BOLD effect is that the coupling of CBF and  $\text{CMRO}_2$  changes could vary across the brain or in disease. If we define  $n$  as the ratio of the fractional changes in CBF and  $\text{CMRO}_2$  with activation, then the physiological basis of the BOLD effect is that  $n > 1$ . However, the exact value of  $n$  plays a significant role in determining the magnitude of the BOLD signal observed for a given underlying metabolic change. In effect, increased CBF acts to wash out deoxyhemoglobin, while increased  $\text{CMRO}_2$  acts to increase local deoxyhemoglobin, so the net change in deoxyhemoglobin depends on the interplay of these two physiological changes. For this reason, the larger the coupling ratio  $n$ , the larger will be the resulting BOLD response for the same change in energy metabolism ( $\text{CMRO}_2$ ). Or, put another way, for two regions with the same change in CBF, the region with the larger change in  $\text{CMRO}_2$  will have a weaker BOLD response. This sensitivity to  $n$  is particularly acute when  $n < 3$ , as a number of studies have found, because theoretical calculations suggest that relatively small differences from  $n = 1.5$  to  $n = 2$ , or from  $n = 2$  to  $n = 3$ , each with the same underlying  $\text{CMRO}_2$  change, will exhibit BOLD responses that differ in magnitude by about 100%.

Cerebral blood flow-based fMRI methods described earlier offer a direct measure of the blood flow response resulting from neural activity, and so can provide information on a more well-defined physiological quantity. At this point it is not clear whether the CBF or the  $\text{CMRO}_2$  change is a better quantitative reflection of the underlying neural activity. Indeed, it is possible that these two responses reflect different aspects of neural activity. Current thinking, although still speculative, is that the CBF response is triggered by excitatory synaptic activity in a feed-forward manner, rather than as a feed-back response due to increased energy demands (Attwell & Iadecola, 2002). In contrast, the  $\text{CMRO}_2$  change likely reflects the full energetic costs of the neural activity, including both synaptic and spiking activity (Attwell & Laughlin, 2001). For these reasons, measures of CBF and  $\text{CMRO}_2$  changes with activation are likely to provide a more accurate reflection of neural function than BOLD alone, and the capability of measuring both physiological responses may be able to provide much more specific quantitative measures of changes in activity.

Davis and colleagues (Davis et al., 1998) proposed the calibrated-fMRI methodology as a means to investigate the nature of neurovascular coupling and the BOLD effect, based on a critical observation. They used an ASL technique to measure both CBF and BOLD responses, and then examined two different types of physiological stimulus. The first was a standard neural activation in response to a particular task, as is commonly done in BOLD-fMRI studies, but the second was the response to increased arterial  $\text{CO}_2$ . Hypercapnia

induced by breathing a gas with 5% CO<sub>2</sub>—approximately equal to the CO<sub>2</sub> content of expired air—has a potent effect of increasing CBF but appears to produce little change in CMRO<sub>2</sub>. They found that for the same change in CBF, the BOLD response was significantly weaker in the neural activation experiment, consistent with increased CMRO<sub>2</sub> with activation.

Based on this observation, they proposed a method for calibrating the BOLD effect in a quantitative way. This approach untangles the three major contributors to the BOLD signal (CBF, CBV, and CMRO<sub>2</sub>) by measuring the CBF and BOLD responses to two challenges; a standardized neural activation experiment, and breathing a gas mixture with an elevated concentration of CO<sub>2</sub>. The hypercapnia experiment is used to isolate and quantify the contribution of known CBF changes to the BOLD signal when there is no change in CMRO<sub>2</sub>. That is, the hypercapnia experiment provides a measurement of the local value of  $M$ , the scaling factor for the BOLD effect. The local CBF and BOLD responses to neural activation are then used in combination with the hypercapnia-calibrated relationship between BOLD and CBF responses and a known relationship between CBF and CBV changes, to estimate the CMRO<sub>2</sub> change with neural activation. The coupling ratio,  $n$ , defined as the ratio of the fractional change in CBF to the fractional change in CMRO<sub>2</sub>, is then easily estimated.

The calibrated-BOLD approach provides a potentially powerful tool for quantitative assessment of the physiological changes following neural activation. In addition to resolving the ambiguities of the BOLD signal noted above, this approach could provide the basis for advancing fMRI from a mapping tool to a quantitative physiological probe for the early assessment of dysfunction in disease. Several groups have adopted this approach and reported values of the CBF/CMRO<sub>2</sub> coupling index  $n$  in the range of 2–4 in several regions of healthy brain; (Davis et al., 1998; Fujita et al., 2006; Hoge et al., 1999b; Kastrup et al., 2002; Kim et al., 1999; Leontiev & Buxton, 2007; St Lawrence et al., 2003; Stefanovic et al., 2005; Stefanovic et al., 2004; Uludag & Buxton, 2004). Other studies have used the framework of the calibrated BOLD approach to argue that CBF and CMRO<sub>2</sub> are coupled in a similar way in deactivations and activations (Shmuel et al., 2002; Stefanovic et al., 2005; Stefanovic et al., 2004; Uludag et al., 2004). A recent paper (Leontiev & Buxton, 2007) has demonstrated that measurement of  $n$  is highly reproducible within a single subject, but more variable across the healthy population, with the population variance measured at about five times the within-subject reproducibility. This suggests that there is a substantial physiological variability that is not understood, but can be probed with these tools.

## Data acquisition and processing

Figure 5 shows an example of data acquired during a calibrated-fMRI experiment. The average CBF and BOLD responses to hypercapnia and a block design visual stimulus are shown. The data were acquired on a 3 Tesla GE whole body system using a dual echo PICORE QUIPSS II ASL sequence with spiral readout (TE = 2.9, 24 ms) (Wong et al., 1997). Simultaneous acquisition has the advantage that any systematic effects over the course of an experiment, such as subject fatigue, affect both the CBF and BOLD measurements in the same way. The data in Fig. 5 are averaged over CBF-active voxels, and are the mean responses over five subjects. Signal to noise ratio constraints mean that CBF and BOLD responses are typically estimated using data averaged over an appropriate region of interest (ROI). Regions of interest are typically defined anatomically or functionally (see following section for a discussion of potential biases in the calculated parameters due to ROI selection).

The model and methods described by Davis et al (Davis et al., 1998) provide a framework for estimating the CMRO<sub>2</sub> changes associated with the measured CBF and BOLD responses. In this model, the fractional BOLD signal change ( $\Delta S/S_0$ ) is related to the underlying changes in CBF and CMRO<sub>2</sub> by the following equation:

$$\frac{\Delta S}{S_0} = M \left[ 1 - \left( \frac{CBF}{CBF_0} \right)^{\alpha-\beta} \left( \frac{CMRO_2}{CMRO_{20}} \right)^\beta \right] \quad (1)$$

where the parameter  $M$  is a proportionality constant that reflects baseline deoxy-hemoglobin content and defines the maximum possible BOLD signal change that would result from a CBF increase sufficiently large to cause 100% venous oxygen saturation. In the context of the model this parameter is proportional to the baseline blood volume fraction, O<sub>2</sub> extraction fraction, the magnetic field strength and the echo time of the experiment. The parameter  $\alpha$  is the exponent in an assumed power law relationship between cerebral blood flow and cerebral blood volume, and is taken to be  $\alpha = 0.38$  (Grubb et al., 1974; Mandeville et al., 1998). The parameter  $\beta$  was introduced as an empirical description of the signal changes found in Monte Carlo simulation studies of spins diffusing near magnetized cylinders, a model for the vascular system (Boxerman et al., 1995b), and usually is taken to be  $\beta = 1.5$  at a field strength of 1.5 Tesla (Boxerman et al., 1995a; Davis et al., 1998). The parameters  $\alpha$  and  $\beta$  are assumed to be global properties with the same values in each subject.

Figure 6 demonstrates the application of the Davis model to measured data. First,  $M$  is estimated from the hypercapnia data using Eq. (1) with the assumption that

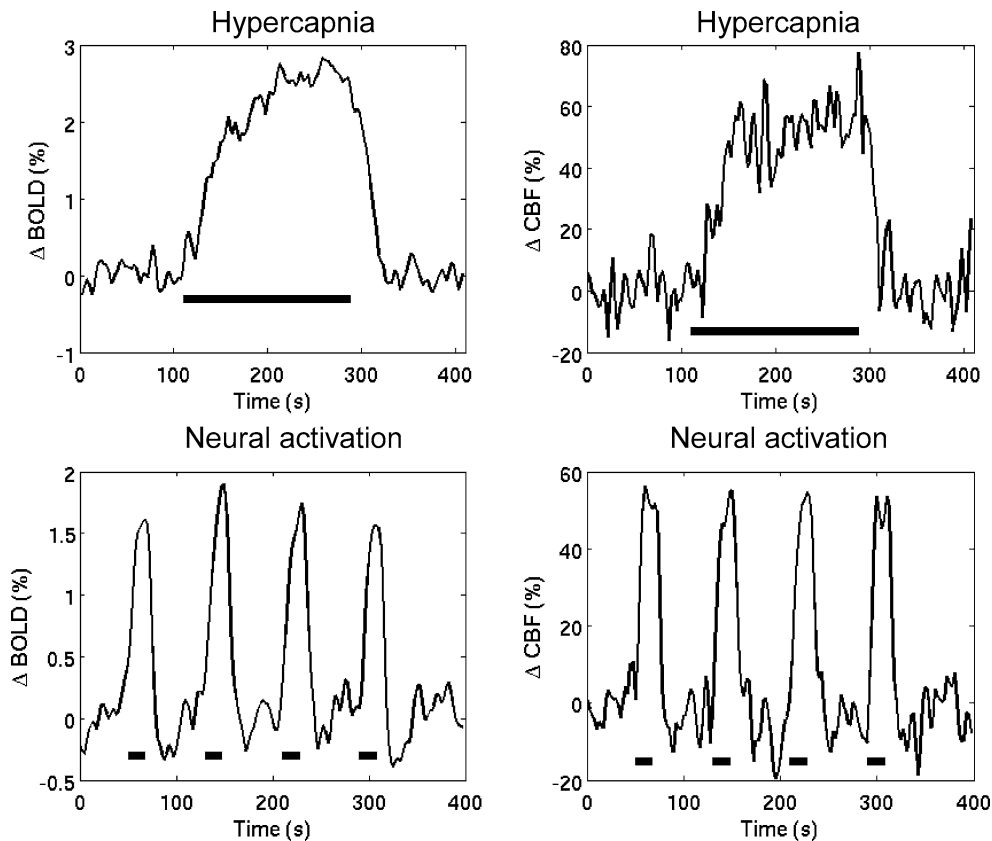


**Fig. 5** Example calibrated-BOLD data (mean data from five subjects). Top row shows the BOLD (left) and CBF (right) responses to a hypercapnic challenge (breathing 5% CO<sub>2</sub>; horizontal bar shows the three minute hypercapnic period). Bottom row shows the mean BOLD (left)

and CBF (right) responses to visual stimulation with a paradigm consisting of a flashing checkerboard presented in four 20 second blocks (horizontal bars depict the “on” periods). BOLD = blood oxygen level dependent; CBF = cerebral blood flow

CMRO<sub>2</sub> = CMRO<sub>20</sub>. Figure 6(a) shows contours of different  $M$  values for measured CBF and BOLD responses to hypercapnia. There have been a wide range of  $M$  values reported in the literature, and  $M$  may vary over different brain regions and therefore should be measured for each experiment. In addition to the estimate of  $M$ , the hypercapnia data provide direct measures of the local vascular responsiveness—the percent change in CBF divided by the change in end-tidal CO<sub>2</sub> (torr)—a measurement that can be used to test for a compromised vascular response in disease.

The BOLD and CBF responses to the neural activation experiment are then used to calculate the fractional change in CMRO<sub>2</sub> in response to functional stimulation by application of Eq. (1) with the value of  $M$  estimated from the hypercapnia experiment. The fractional change in CMRO<sub>2</sub>, combined with the measured fractional change in CBF, gives an estimate of  $n$ . Figure 6(b) shows contours of different  $n$  values for measured CBF and BOLD responses to neural activation, assuming a value for  $M$  of 8%. Note that a measurement of  $n = 1$  (equal fractional changes in CBF and CMRO<sub>2</sub> to stimulation) requires the measurement of a positive CBF response and a negative BOLD response (or vice versa), due to the form of the Davis model. Figure 6(c) shows

the same data, but also shows the effect of a change in  $M$  on the  $n$  contours. The contours get squeezed together in CBF-BOLD space as  $M$  reduces.

#### Limitations and sources of bias in calibrated-blood oxygen level dependant experiments

For estimating physiological quantities such as CMRO<sub>2</sub> changes and  $n$ , it is critical to apply a consistent methodology that minimizes bias in the measurements. Some factors requiring consideration in any calibrated-BOLD study are described below.

#### Calibrated-BOLD assumptions

##### *Does mild hypercapnia alter CMRO<sub>2</sub>?*

A key assumption of the calibrated BOLD approach is that inhalation of air with added CO<sub>2</sub> increases CBF but does not change CMRO<sub>2</sub>. A number of early studies support this assumption (Horvath et al., 1994; Kety & Schmidt, 1948; Novack et al., 1953; Yang & Krasny, 1995), but it remains a controversial issue. Recent work in rodents found that 5%

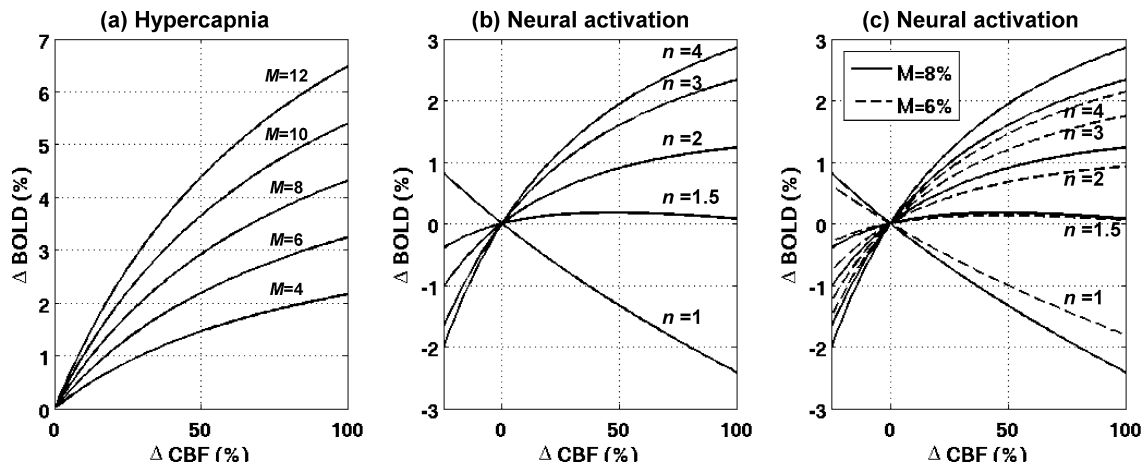


**Fig. 6** The Davis model. (a) Measured CBF and BOLD responses to hypercapnia are used to determine the local BOLD scaling parameter  $M$ , assuming no  $\text{CMRO}_2$  change. Contours of  $M$  values of 4–12% are shown. (b) Measured CBF and BOLD responses to neural activation are used in combination with  $M$  to determine the CBF/ $\text{CMRO}_2$  coupling

ratio  $n$  ( $M = 8\%$  in this example). Contours of  $n$  values from 1–4 are shown. (c) Contours of  $n$  values for  $M = 6\%$  are included in addition to the  $M = 8\%$  data to show the compression of the contours as  $M$  decreases. BOLD = blood oxygen level dependent; CBF = cerebral blood flow

hypercapnia produced negligible changes in  $\text{CMRO}_2$  whereas 10% produced significant changes (Jones et al., 2005; Sicard & Duong, 2005). However, a recent study (Zappe et al., 2005) reported decreases in electrophysiological measures in anesthetized macaques with 3 and 6%  $\text{CO}_2$ . If these correlate with  $\text{CMRO}_2$ , this would imply decreased  $\text{CMRO}_2$  with hypercapnia, which in turn would suggest that calibrated BOLD techniques overestimate  $\text{CMRO}_2$  and underestimate  $n$ . However, it is not clear in these animal experiments how anesthesia interacts with the  $\text{CO}_2$ , and we need to be cautious when interpreting electrophysiology in terms of energy metabolism. The question is complicated because we would expect that at higher concentrations  $\text{CO}_2$  has an anesthetic effect, and would be expected to reduce  $\text{CMRO}_2$ . More work is needed in this area, but for the moment there is good evidence to suggest that mild hypercapnia does not significantly violate the assumptions of the calibrated-BOLD approach.

#### Davis model foundations

Equation (1) represents the central model used in the calibrated BOLD approach. At first glance, it may appear to be too simplistic, because the original simulations that led to this equation did not include the contribution of intravascular signal changes to the BOLD signal. At lower magnetic field strengths (including 3 Tesla) the intravascular and extravascular contributions to the net signal changes are expected to be comparable (Boxerman et al., 1995a). While the extravascular signal changes primarily depend on changes in the *total* deoxy-hemoglobin, the intravascular signal changes depend on changes in the deoxy-hemoglobin *concentration* within blood. In addition, intravascular volume changes also affect

the signal when the intrinsic intra- and extra-vascular signals are different, creating signal changes due to the exchange of compartmental volumes. (Buxton et al., 2004; Buxton et al., 1998; Obata et al., 2004). However, when curves of BOLD response versus CBF response are calculated with the more complete model that includes these other effects (Obata et al., 2004), Eq. (1) still provides a close approximation (Buxton et al., 2004). That is, despite the apparently oversimplified assumptions that led to Eq. (1), it nevertheless captures the basic behavior expected for a BOLD response that includes both an extravascular and an intravascular contribution to the BOLD effect. The key to this is that  $\beta > 1$ , the practical effect of which is that the BOLD signal change is not a pure linear function of local deoxyhemoglobin content (it would be if  $\beta = 1$ ) (Buxton et al., 2004). In short, the Davis model is likely to be more robust than one would have imagined given the simple assumptions it was originally based on. However, this more complex interpretation of the net BOLD effect also suggests that the parameter  $M$  cannot be estimated from first principles (i.e., from the original derivation of Eq. (1)), because it also must partly reflect the role of intravascular signal changes. For this reason  $M$  must be measured in each experiment.

#### Data processing considerations

##### Selecting an ROI

In principle, the measurement of CBF and BOLD responses to hypercapnia and neural stimulation could be performed on a voxel by voxel basis, but SNR constraints mean that the responses are typically estimated using data averaged over an ROI. A recent study (Leontiev et al., submitted) has

investigated the impact of different methods for choosing an ROI, comparing CMRO<sub>2</sub> and *n* values obtained in response to a visual stimulus using ROIs based on: 1) retinotopically-defined area V1; 2) a functional CBF localizer; and 3) a functional BOLD localizer. Data in V1 yielded a significantly lower estimate of *n* compared to either CBF or BOLD localizers. In addition, different statistical thresholds for defining active voxels produced biases in the estimates of *n*, with the estimated value increasing for higher thresholds. This study highlighted a potential source of bias in anatomically-defined ROIs. Since hypercapnia induces a global CBF response, every venous structure in the anatomically defined ROI acts as a draining vein. The measured BOLD response to hypercapnia may therefore be artifactually large due to the inclusion of draining veins within the ROI. This propagates into an overestimation of *M* and underestimation of *n*. Therefore, although it seems like using an anatomical ROI is a good idea because it is unbiased with regard to functional activity, in fact it may bring in a significant bias in the calculation of CBF/CMRO<sub>2</sub> coupling by inclusion of draining veins, which has a strong effect on the average BOLD response to CO<sub>2</sub>.

It should also be noted that the form of the Davis model itself also places restrictions on the measured *n* value under certain ROI choices. As can be seen in Fig. 6(b), an ROI consisting of only those voxels that show a positive BOLD and CBF response, have to produce a measured *n* greater than about 1.4.

#### *Inclusion/exclusion of the BOLD post-stimulus undershoot*

A common phenomenon observed in BOLD-fMRI studies is a pronounced post-stimulus undershoot of the BOLD signal. This observation has been puzzling because there is often no corresponding undershoot of CBF, suggesting in these cases a transient uncoupling of one or more of the other physiological factors that contribute to the BOLD response. This phenomenon may be the result of a biomechanical effect that leads to a slow return of blood volume to baseline (Buxton et al., 1998; Mandeville et al., 1999b), or may be due to a slower return of CMRO<sub>2</sub> to baseline than CBF, requiring increased O<sub>2</sub> extraction and creating increased local deoxyhemoglobin (Frahm et al., 1996). There is currently no consensus in the literature, leaving the question of how the undershoot should be treated in the analysis of CBF/CMRO<sub>2</sub> coupling. If it is due to slow CBV recovery, then during the undershoot period the BOLD response is no longer reflecting CBF/CMRO<sub>2</sub> coupling and so this period should be excluded from the analysis. However, if the undershoot *does* reflect a slow recovery of CMRO<sub>2</sub>, then it would be important to include the undershoot period in the calculations for a full accounting of the CMRO<sub>2</sub> change.

Davis model limitations: Overestimates of *M* create artifactually low estimates of *n*

In a recent paper, Chiarelli and colleagues (Chiarelli et al., 2007) show that over or under estimation of *M* can introduce significant bias into the value of *n*. In particular, if the estimate of *M* is artifactually high, then regardless of the actual BOLD activation measurement the estimate of *n* is driven to low values. The source of this effect can be seen by re-arranging the Davis equation:

$$\left(\frac{\text{CMRO}_2}{\text{CMRO}_{20}}\right)^\beta = \left(\frac{\text{CBF}}{\text{CBF}_0}\right)^{\beta-\alpha} \left[1 - \left(\frac{\Delta S/S_0}{M}\right)\right] \quad (2)$$

If the BOLD response to neural activation is small in comparison to *M* (i.e. the BOLD response to activation is much less than the BOLD response to hypercapnia), the term in square brackets in Eq. (2) approaches 1, and the estimate of *n* is driven toward *n* ~ 1.4 (Chiarelli et al., 2007). This can also be seen in Fig. 6(c), where small BOLD responses lead to *n* ~ 1.4, and as *M* increases, the *M* contours move apart such that *n* is driven towards 1.4 regardless of the measured BOLD signal. See Chiarelli and colleagues paper for a further discussion of this issue (Chiarelli et al., 2007).

#### Potential applications

A calibrated-BOLD approach offers a potentially powerful paradigm for fMRI: rather than using fMRI simply as a mapping tool, we can instead use it as a quantitative probe of brain physiology analogous to a “stress test.” That is, we can stimulate a particular brain region with a stereotyped stimulus and measure the local CBF and CMRO<sub>2</sub> responses to the activation as well as the CBF response to CO<sub>2</sub>. For clinical applications, the calibrated-BOLD approach offers the possibility of a more quantitative and comprehensive evaluation of brain function than is possible with BOLD-fMRI alone. We still know relatively little about how the coupling of CBF and CMRO<sub>2</sub> varies in the healthy brain. A deeper understanding of the links between neural activity and energy metabolism, and the role played by blood flow, will provide a framework for understanding the mechanisms of disease. The hypothesized links between neurodegenerative diseases and mitochondria (Ly & Verstreken, 2006; Moncada & Bolanos, 2006) suggest that energy metabolism may play an important role in a number of disease processes, but these connections are still unclear. General tools for assessing human brain physiology in a quantitative way could be useful for early detection of disease, quantifying response to therapy, evaluating drug effects and investigation of the mechanisms of disease.

As an illustration of the potential application of the calibrated BOLD approach in resolving intrinsic ambiguities

of the BOLD response, suppose that a study finds a weaker BOLD response to a particular task in a group of test subjects compared to controls (e.g., a weaker BOLD response in hippocampus to a memory task in early Alzheimer's disease subjects compared to healthy controls): how should this be interpreted? Figure 7 illustrates some possibilities. A measured decrease in the BOLD response to neural activation might naively be interpreted as a decrease in neural activity and therefore a coupled decrease in CBF and CMRO<sub>2</sub>. While this may indeed be the case (see Fig. 7(a)), other scenarios are possible in which the BOLD decrease may not in fact be associated with a decrease in CMRO<sub>2</sub>. As shown in Fig. 7(b), a decrease in the CBF/CMRO<sub>2</sub> coupling ratio  $n$ , perhaps caused by a compromised CBF response, could also cause a weaker BOLD response (this effect might also be evident in a reduced CBF response to CO<sub>2</sub>). Furthermore, as shown in Fig. 7(c), a weaker BOLD response may result from a decrease in  $M$ , perhaps caused by an increase in baseline CBF due to medications used by the test subject group. See Wierenga and Bondi (2007) in this volume for an example of the impact of unequal  $M$  when comparing the BOLD response of individuals of different ages. A BOLD-only experiment clearly cannot resolve these three scenarios. Although a combined BOLD and CBF experiment provides more data, a calibrated fMRI approach is required to fully distinguish among the interpretative possibilities.

Recent work suggests that the CBF/CMRO<sub>2</sub> coupling ratio  $n$  may be smaller in deeper brain structures than in cortex. This suggests the possibility that neural activity changes of the same magnitude may be significantly easier to detect in some brain structures than in others. Or to put it another way, a map of activation highlighting those voxels with a significant correlation of the BOLD response with the task could miss areas of brain with a similar level of activity but a lower coupling ratio  $n$ . This highlights an important aspect of the statistical analysis used to produce maps of activation: the emphasis is to avoid false positives, rather than false negatives. Combined measurement of BOLD and CBF responses, particularly in the context of a calibrated-BOLD experiment, can help to unravel these ambiguities of the BOLD response. The use of calibrated-BOLD methodology is still in its infancy, but the potential is high for this approach to provide a more quantitative and specific characterization of brain function in health and disease.

#### Functional MRI: Issues relevant to clinical practice

Functional MRI is a non-invasive, highly repeatable technique. Its spatial resolution and capacity to localize is generally better than what can be obtained in human lesion studies. Although its temporal resolution is one to two orders of magnitude slower than most neural events, its time scale is appropriate for some behavioral processes, such as

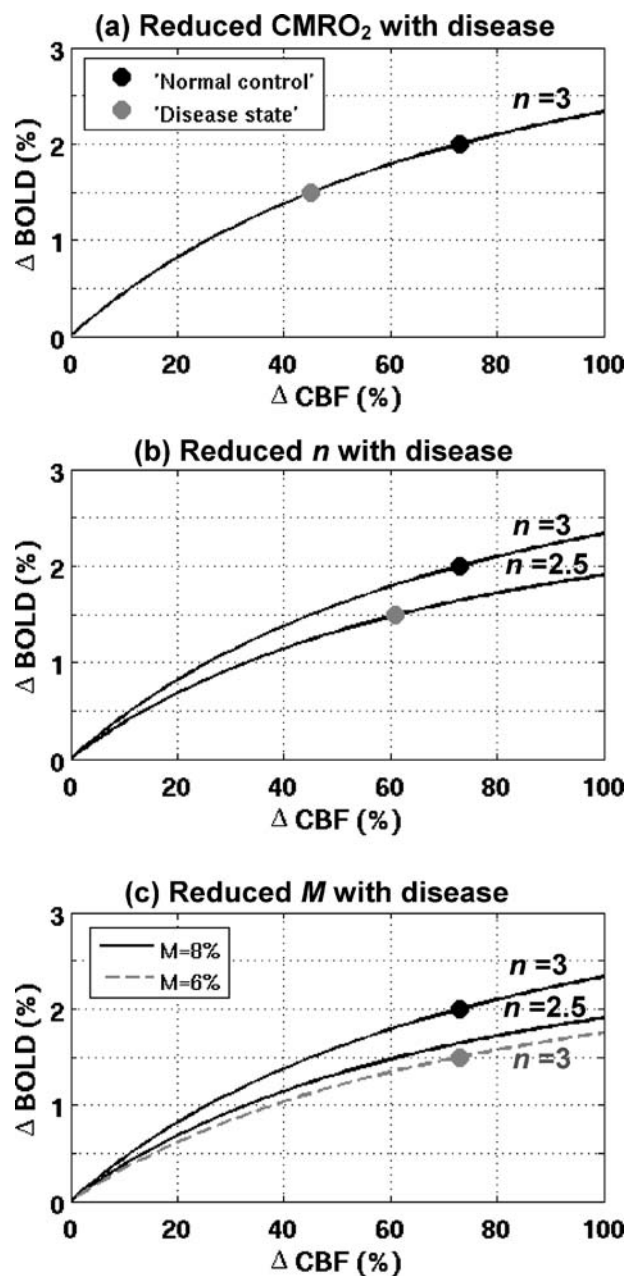


**Fig. 7** Three physiological scenarios leading to a decrease in the BOLD response to neural activation in a ‘disease’ population compared to a ‘normal’ population, each showing a 2% BOLD response in the ‘normal’ condition and a 1.5% BOLD response in the “disease” condition. In this example, the normal condition has  $M = 8\%$  and  $n = 3$ . In (a), the BOLD response reduction is due to a reduction in neural activity in the disease state, but with a normal CBF/CMRO<sub>2</sub> coupling ratio  $n$ . In (b), the CBF response is compromised but the neural activity and CMRO<sub>2</sub> changes are maintained, resulting in a reduction in  $n$ . In (c), baseline CBF is elevated whilst baseline CMRO<sub>2</sub>, neural activity and  $n$  remain constant. This causes a decrease in  $M$ , leading to the reduced BOLD response. Thus an identical difference in the BOLD response between groups can arise in three very different ways. Although combined BOLD and CBF data can begin to resolve the ambiguities, calibrated fMRI with estimation of  $M$  and  $n$  is required to obtain a more complete interpretation of the data. BOLD = blood oxygen level dependent; CBF = cerebral blood flow

verbal rehearsal (Rundus, 1971). A considerable strength of fMRI methods is its availability. A 2004 survey reported approximately 5,000 magnetic resonance imaging sites in the United States compared with 1500 sites supporting positron emission tomography (Latest IMV PET 2004; Latest IMV Study, 2005). Currently shipped magnets from all major vendors have fMRI capability. High field magnetic resonance imaging systems are being sited in Psychology and Cognitive Science Departments, making them more available to academic psychologists.

The magnitude of the BOLD response is small, usually between 0.25% and 5.0%. Although the small size of the signal would not be an issue if the sources of noise were much smaller, noise and bias are significant problems for the fMRI experiment. The baseline signal drifts over the several minutes of a run. Heating of the system amplifiers and other electronic components can produce moment-to-moment changes in system performance. Subject motivation and attention vary from trial to trial. Neural systems habituate to or learn from repeated stimulation. The BOLD method is sensitive to movement, which especially produces edge artifacts. Both behavioral and physiological sources of movement, such as respiration or cardiac cycles, are common. Movement is especially troublesome if it correlates with stimulus changes (Hajnal et al., 1995). Generally, fMRI researchers coregister images collected across the time series to a base image in order to reduce the impact of movement. These adjustments can correct small misalignments due to movement but do not adjust the signal for loss of phase when spins at a brain location experience slightly different magnetic fields as they move throughout the experiment (Buxton, 2002). As described above, the bulk of the BOLD signal at commonly used field strengths originates within and around veins. The location of the venous contribution of the BOLD signal can be as much as a centimeter removed for the capillary bed supplying the activated brain tissue (Kwong et al., 1995). Whereas movement can cause artifactual BOLD signals, the brain-vein problem mislocates the BOLD signal. Areas of the brain where the proximity of different tissue compartments produces a gradient of tissue susceptibilities, such as the orbitofrontal cortex or the temporal cortex adjacent to the auditory canal, experience signal loss and mislocation of image voxels.

The BOLD signal is physiologically non-specific, as it depends on baseline cerebral blood volume and metabolism and on cerebrovascular reactivity, in addition to task related changes of oxygen utilization. This lack of physiological specificity is especially challenging for studies of drugs that may alter baseline cerebral blood flow or drugs, such as caffeine, that alter the shape of the hemodynamic response (Brown et al., 2003; Liu et al., 2004). The effect of pharmacological treatments on cerebral vessels should be considered when analyzing BOLD data from

treated patients or from drug development studies (See the Paulus and Stein article in this issue). Sophisticated modeling of the BOLD response is needed to disentangle the various physiological contributions to the BOLD signal.

Details of the behavioral activation paradigm affect the efficiency of a BOLD study. These details include appropriate design of the experimental task and effective selection of items to study. Together task design and item selection determine the reliability and power of a behavioral paradigm used to activate brain processes. Likewise, details of the image analysis pathway and the statistical modeling of MR time series signals can have considerable effect on the dependability of fMRI results. To produce dependable results in individual cases, careful standardization, which has been a hallmark of psychological testing, will need to be developed for fMRI assessments.

**Acknowledgements** Preparation of this paper was supported by the VISN 22 Mental Illness Research Education and Clinical Center, a Biomedical Engineering Research Grant from the Whitaker Foundation, and by NIH grants #1 U24 RR021992 to the Function Biomedical Informatics Research Network (FBIRN, <http://www.nbirn.net>), 1 RO1 NS051661 to Thomas Liu, and 1 RO1 NS051661 and 1 RO1 NS367220 to Richard Buxton.

## References

- Aguirre, G. K., Detre, J. A., & Wang, J. (2005). Perfusion fMRI for functional neuroimaging. *International Review of Neurobiology*, 66, 213–236.
- Aguirre, G. K., Detre, J. A., Zarahn, E., & Alsop, D. C. (2002). Experimental design and the relative sensitivity of BOLD and perfusion fMRI. *NeuroImage*, 15, 488–500.
- Aguirre, G. K., Zarahn, E., & D'esposito, M. (1998). The variability of human, BOLD hemodynamic responses. *NeuroImage*, 8, 360–369.
- Alsop, D. C. (2006). Perfusion imaging of the brain: Contribution to clinical MRI. In R. R. Edelman, J. R. Hesselink, M. B. Zlatkin, & J. V. Cures III (Eds.), *Clinical magnetic resonance imaging* (3rd edn., Vol. 1, pp. 333–357). Philadelphia: Saunders Elsevier.
- Attwell, D., & Iadecola, C. (2002). The neural basis of functional brain imaging signals. *Trends in Neurosciences*, 25, 621–625.
- Attwell, D., & Laughlin, S. B. (2001). An energy budget for signaling in the grey matter of the brain. *Journal of Cerebral Blood Flow and Metabolism*, 21, 1133–1145.
- Bandettini, P. A., Wong, E. C., Hinks, R. S., Tikofsky, R. S., & Hyde, J. S. (1992). Time course EPI of human brain function during task activation. *Magnetic Resonance in Medicine*, 25, 390–397.
- Bandettini, P. A., & Cox, R. W. (2000). Event-related fMRI contrast when using constant interstimulus interval: Theory and experiment. *Magnetic Resonance in Medicine*, 43, 540–548.
- Berger, T. W. (1984). Neural representation of associative learning in the hippocampus. In L. R. Squire & N. Butters (Eds.), *Neuropsychology of memory* (pp. 443–461). New York: The Guilford Press.
- Boxerman, J. L., Bandettini, P. A., Kwong, K. K., Baker, J. R., Davis, T. L., Rosen, B. R., & Weisskoff, R. M. (1995a). The intravascular contribution to fMRI signal change: Monte Carlo modeling and diffusion-weighted studies in vivo. *Magnetic Resonance in Medicine*, 34, 4–10.

- Boxerman, J. L., Hamberg, L. M., Rosen, B. R., & Weisskoff, R. M. (1995b). MR contrast due to intravascular magnetic susceptibility perturbations. *Magnetic Resonance in Medicine*, 34, 555–566.
- Boynton, G. M., Engel, S. A., Glover, G. H., & Heeger, D. J. (1996). Linear systems analysis of functional magnetic resonance imaging in humans. *The Journal of Neuroscience*, 16, 4207–4221.
- Brown, G. G., Eyler Zorrilla, L. T., Georgy, B., Kindermann, S. S., Wong, E. C., & Buxton, R. B. (2003). BOLD and perfusion response to finger-thumb apposition after acetazolamide administration: Differential relationship to global perfusion. *Journal of Cerebral Blood Flow and Metabolism*, 23, 829–837.
- Burock, M. A., Buckner, R. L., Woldorff, M. G., Rosen, B. R., & Dale, A. M. (1998). Randomized event-related experimental designs allow for extremely rapid presentation rates using functional MRI. *NeuroReport*, 9, 3735–3739.
- Buxton, R. B. (2002). *Introduction to functional magnetic resonance imaging*. Cambridge: Cambridge University Press.
- Buxton, R. B., Uludag, K., Dubowitz, D. J., & Liu, T. T. (2004). Modeling the hemodynamic response to brain activation. *Neuroimage*, 23(Suppl. 1), 220–233.
- Buxton, R. B., Wong, E. C., & Frank, L. R. (1998). Dynamics of blood flow and oxygenation changes during brain activation: the balloon model. *Magnetic Resonance in Medicine*, 39, 855–864.
- Chiarelli, P., Bulte, D. P., Piechnik, S., & Jezzard, P. (2007). Sources of systematic bias in hypercapnia-calibrated functional MRI estimation of oxygen metabolism. *NeuroImage*, 34, 35–43.
- Cohen, M. S. (1997). Parametric analysis of fMRI data using linear systems methods. *NeuroImage*, 6, 93–103.
- Dale, A. M. (1999). Optimal experimental design for event-related fMRI. *Human Brain Mapping*, 8, 109–114.
- Dale, A. M., & Buckner, R. L. (1997). Selective averaging of rapidly presented individual trials using fMRI. *Human Brain Mapping*, 5, 329–340.
- Daniels, F., & Albert, R. A. (1966). *Physical chemistry* (3rd edn.). New York: John Wiley & Sons.
- Davis, T. L., Kwong, K. K., Weisskoff, R. M., & Rosen, B. R. (1998). Calibrated functional MRI: Mapping the dynamics of oxidative metabolism. *Proceedings of the National Academy of Science USA*, 95, 1834–1839.
- Detre, J. A., Leigh, J. S., Williams, D. S., & Koretsky, A. P. (1992). Perfusion imaging. *Magnetic Resonance in Medicine*, 23, 37–45.
- Donaldson, D. I., & Buckner, R. L. (2001). Effective paradigm design. In P. Jezzard, P. M. Matthews, & S. M. Smith (Eds.), *Functional MRI: An Introduction to methods* (pp. 177–195). New York: Oxford University Press.
- Edelman, R. R., Siewert, B., Darby, D. G., Thangaraj, V., Nobre, A. C., Mesulam, M. M., & Warach, S. (1994). Qualitative mapping of cerebral blood flow and functional localization with echo-planar MR imaging and signal targeting with alternating radio frequency. *Radiology*, 192, 513–520.
- Elster, A. D., & Burdette, J. H. (2001). *Questions & answers in magnetic resonance imaging* (2nd edn.). St. Louis: Mosby.
- Frahm, J., Krüger, G., Merboldt, K.-D., & Kleinschmidt, A. (1996). Dynamic uncoupling and recoupling of perfusion and oxidative metabolism during focal activation in man. *Magnetic Resonance in Medicine*, 35, 143–148.
- Friston, K. J., Josephs, O., Rees, G., & Turner, R. (1998). Non-linear event-related responses in fMRI. *Magnetic Resonance in Medicine*, 39, 41–52.
- Friston, K. J., Price, C. J., Fletcher, P., Moore, C., Frackowiak, R. S. J., & Dolan, R. J. (1996). The trouble with cognitive subtraction. *NeuroImage*, 4, 97–104.
- Fujita, N., Matsumoto, K., Tanaka, H., Watanabe, Y., & Murase, K. (2006). Quantitative study of changes in oxidative metabolism during visual stimulation using absolute relaxation rates. *NMR in Biomedicine*, 19, 60–68.
- Garcia, D. M., Bazelaire, C. D., & Alsop, D. (2005). *Pseudo-continuous flow drive adiabatic inversion for arterial spin labeling*. Paper presented at the 13th ISMRM Scientific Meeting, Miami Beach.
- Gjedde, A. (2001). Brain energy metabolism and the physiological basis of the haemodynamic response. In P. Jezzard, P. M. Matthews, & S. M. Smith (Eds.), *Functional MRI: An Introduction to methods* (pp. 37–65). New York: Oxford University Press.
- Grubb, R. L., Raichle, M. E., Eichling, J. O., & Ter-Pogossian, M. M. (1974). The effects of changes in PaCO<sub>2</sub> on cerebral blood volume, blood flow, and vascular mean transit time. *Stroke*, 5, 630–639.
- Guyton, A. C. (1977). *Basic human physiology: Normal function and mechanisms of disease* (2nd edn.). Philadelphia: W.B. Saunders Company.
- Hajnal, J. V., Bydder, G. M., & Young, I. R. (1995). fMRI: Does correlation imply activation. *NMR in Biomedicine*, 8, 97–100.
- Hoge, R. D., Atkinson, J., Gill, B., Crelier, G. R., Marrett, S., & Pike, G. B. (1999). Linear coupling between cerebral blood flow and oxygen consumption in activated human cortex. *Proceedings of the National Academy of Science USA*, 96(16), 9403–9408.
- Horvath, I., Sandor, N. T., Ruttner, Z., & McLaughlin, A. C. (1994). Role of nitric oxide in regulating cerebrocortical oxygen consumption and blood flow during hypercapnia. *Journal of Cerebral Blood Flow and Metabolism*, 14, 503–509.
- Huettel, S. A., Song, A. W., & McCarthy, G. (2004). *Functional Magnetic Resonance Imaging*. Sunderland, MA: Sinauer Associates.
- Hyder, F. (2004). Neuroimaging with calibrated fMRI. *Stroke*, 35(Suppl 1), 2635–2641.
- Jezzard, P., Matthews, P. M., & Smith, S. M. (Eds.). (2001). *Functional MRI: An Introduction to methods*. New York: Oxford University Press.
- Jones, M., Berwick, J., Hewson-Stoate, N., Gias, C., & Mayhew, J. (2005). The effect of hypercapnia on the neural and hemodynamic responses to somatosensory stimulation. *Neuroimage*, 27, 609–623.
- Karu, Z. Z. (1995). *Signals and systems made ridiculously simple*. Cambridge, MA: ZiZi Press.
- Kastrup, A., Kruger, G., Neumann-Haefelin, T., Glover, G. H., & Moseley, M. E. (2002). Changes of cerebral blood flow, oxygenation, and oxidative metabolism during graded motor activation. *Neuroimage*, 15, 74–82.
- Kemeny, S., Ye, F. Q., Birn, R., & Braun, A. R. (2005). Comparison of continuous overt speech fMRI using BOLD and arterial spin labeling. *Human Brain Mapping*, 24, 173–183.
- Kety, S. S., & Schmidt, C. F. (1948). The effects of altered arterial tensions of carbon dioxide and oxygen on cerebral blood flow and cerebral oxygen consumption of normal young men. *The Journal of Clinical Investigation*, 27, 484–492.
- Kim, S. G., Rostrup, E., Larsson, H. B. W., Ogawa, S., & Paulson, O. B. (1999). Determination of relative CMRO<sub>2</sub> from CBF and BOLD changes: significant increase of oxygen consumption rate during visual stimulation. *Magnetic Resonance in Medicine*, 41, 1152–1161.
- Kim, S.-G., & Tsekos, N. V. (1997). Perfusion imaging by a flow-sensitive alternating inversion recovery (FAIR) technique: Application to functional brain imaging. *Magnetic Resonance in Medicine*, 37, 425–435.
- Kwong, K. K., Chesler, D. A., Weisskoff, R. M., Donahue, K. M., Davis, T. L., Ostergaard, L., Campbell, T. A., & Rosen, B. R. (1995). MR perfusion studies with T1-weighted echo planar imaging. *Magnetic Resonance in Medicine*, 34, 878–887.
- Latest IMV PET census shows fast growth in PET/CT installations. 2004 (Nov. 18). *News from IMV's Medical Information Division*. [http://www.imvlimited.com/mid/news\\_c.html](http://www.imvlimited.com/mid/news_c.html).

- Latest IMV study shows MRI clinical utilization expanding. 2005 (Feb. 19). *News from IMV's Medical Information Division*. [http://www.imvlimited.com/mid/news\\_a.html](http://www.imvlimited.com/mid/news_a.html).
- Leontiev, O., & Buxton, R. B. (2007). Reproducibility of BOLD, perfusion, and CMRO<sub>2</sub>(2) measurements with calibrated-BOLD fMRI. *NeuroImage*, 35, 175–184.
- Leontiev, O., Dubowitz, D. J., & Buxton, R. B. (2007). *CBF/CMRO<sub>2</sub> coupling measured with calibrated-BOLD fMRI: Sources of bias*. Manuscript submitted for publication.
- Liu T. T. (2004). Efficiency, power, and entropy in event-related fMRI with multiple trial types. Part II: Design of experiments. *NeuroImage*, 21, 401–413.
- Liu T. T., Behzadi, Y., Restom, K., Uludag, K., Lu, K., Buracas, G. T., Dubowitz, D. J., & Buxton, R. B. (2004). Caffeine alters the temporal dynamics of the visual BOLD response. *NeuroImage*, 23, 1402–1413.
- Liu, T. T., & Brown, G. G. (2007). Measurement of cerebral perfusion with arterial spin labeling: Part 1. methods. *Journal of the International Neuropsychological Society*.
- Liu T. T., & Frank, L. R. (2004). Efficiency, power, and entropy in event-related fMRI with multiple trial types. Part I: Theory. *NeuroImage*, 21, 387–400. Erratum in *NeuroImage* (2004), 22, 1427.
- Liu, T. T., Frank, L. R., Wong, E. C., & Buxton, R. B. (2001). Detection power, estimation efficiency, and predictability in event-related fMRI. *NeuroImage*, 13, 759–773.
- Liu, T. T., & Wong, E. C. (2005). A signal processing model for arterial spin labeling functional MRI. *NeuroImage*, 24, 207–215.
- Liu, T. T., Wong, E. C., Frank, L. R., & Buxton, R. B. (2002). Analysis and design of perfusion-based event-related fMRI experiments. *NeuroImage*, 16, 269–282.
- Ly, C. V., & Verstreken, P. (2006). Mitochondria at the synapse. *Neuroscientist*, 12, 291–299.
- Mandeville, J. B., Marota, J. J. A., Ayata, C., Zaharchuk, G., Moskowitz, M. A., Rosen, B. R., & Weisskoff, R. M. (1999b). Evidence of a cerebrovascular post-arteriole Windkessel with delayed compliance. *Journal of Cerebral Blood Flow and Metabolism*, 19, 679–689.
- Mandeville, J. B., Marota, J. J. A., Kosofsky, B. E., Keltner, J. R., Weissleder, R., Rosen, B. R., & Weisskoff, R. M. (1998). Dynamic functional imaging of relative cerebral blood volume during rat forepaw stimulation. *Magnetic Resonance in Medicine*, 39, 615–624.
- Mildner, T., Zysset, S., Trampel, R., Driesel, W., & Möller, H. E. (2005). Towards quantification of blood-flow changes during cognitive task activation using perfusion-based fMRI. *NeuroImage*, 27, 919–926.
- Miller, K. L., Luh, W. M., Liu, T. T., Martinez, A., Obata, T., Wong, E. C., Frank, L. R., & Buxton, R. B. (2001). Nonlinear temporal dynamics of the cerebral blood flow response. *Human Brain Mapping*, 13, 1–12.
- Moncada, S., & Bolanos, J. P. (2006). Nitric oxide, cell bioenergetics and neurodegeneration. *Journal of Neurochemistry*, 97, 1676–1689.
- Mumford, J. A., Hernandez-Garcia, L., Lee, G. R., & Nichols, T. A. (2006) Estimation efficiency and statistical power in arterial spin labeling fMRI. *NeuroImage*, 33, 103–114.
- Novack, P., Shenkin, H. A., Bortin, L., Goluboff, B., & Sofie, A. M. (1953). The effects of carbon dioxide inhalation upon the cerebral blood flow and cerebral oxygen consumption in vascular disease. *The Journal of Clinical Investigation*, 32, 696–702.
- Obata, T., Liu, T. T., Miller, K. L., Luh, W. M., Wong, E. C., Frank, L. R., & Buxton, R. B. (2004). Discrepancies between BOLD and flow dynamics in primary and supplementary motor areas: application of the balloon model to the interpretation of BOLD transients. *NeuroImage*, 21, 144–153.
- Ogawa, S., Tso-Ming, L., Nayak, A. S., & Glynn, P. (1990). Oxygen-sensitive contrast in magnetic resonance image of rodent brain at high magnetic fields. *Magnetic Resonance in Medicine*, 14, 68–78.
- Ogawa, S., Menon, R. S., Tank, D. W., Kim, S.-G., Merkle, H., Ellerman, J. M., & Ugurbil, K. (1993). Functional brain mapping by blood oxygenation level-dependent contrast magnetic resonance imaging: A comparison of signal characteristics with a biophysical model. *Biophysical Journal*, 64, 803–812.
- Rao, S. M., Salmeron, B. J., Durgerian S., Janowiak, J. A., Fischer, M., Risinger, R. C., Conant, L. L., & Stein, E. A. (2000). Effects of methylphenidate on functional MRI blood-oxygen-level-dependent contrast. *American Journal of Psychiatry*, 157, 1697–1699.
- Restom, K., Behzadi, Y., & Liu, T. T. (2006). Physiological noise reduction for arterial spin labeling functional MRI. *NeuroImage*, 31, 1104–1115.
- Rundus, D. (1971). Analysis of rehearsal processes in free recall. *Journal of Experimental Psychology*, 89, 63–77.
- Shmuel, A., Yacoub, E., Pfeuffer, J., Van de Moortele, P. F., Adriany, G., Hu, X., Ugurbil, K. (2002). Sustained negative BOLD, blood flow and oxygen consumption response and its coupling to the positive response in the human brain. *Neuron*, 36, 1195–1210.
- Sicard, K. M., & Duong, T. Q. (2005) Effects of hypoxia, hyperoxia, and hypercapnia on baseline and stimulus-evoked BOLD, CBF, and CMRO<sub>2</sub> in spontaneously breathing animals. *NeuroImage*, 25, 850–858.
- St Lawrence, K. S., Ye, F. Q., Lewis, B. K., Frank, J. A., & McLaughlin, A. C. (2003). Measuring the effects of indomethacin on changes in cerebral oxidative metabolism and cerebral blood flow during sensorimotor activation. *Magnetic Resonance in Medicine*, 50, 99–106.
- Stefanovic, B., Warnking, J. M., Kobayashi, E., Bagshaw, A. P., Hawco, C., Dubeau, F., Gotman, J., & Pike, G. B. (2005). Hemodynamic and metabolic responses to activation, deactivation and epileptic discharges. *NeuroImage*, 28, 205–215.
- Stefanovic, B., Warnking, J. M., & Pike, G. B. (2004). Hemodynamic and metabolic responses to neuronal inhibition. *NeuroImage*, 22, 771–778.
- Sternberg, S. (1969). The discovery of processing stages: Extension of Donders method. *Acta Psychologica*, 30, 276–315.
- Thulborn, K. R., Waterton, J. C., Matthews, P. M., & Rada, G. K. (1982). Oxygenation dependence of the transverse relaxation time of water protons in whole blood at high field. *Biochimica et Biophysica Acta*, 714, 265–270.
- Tjandra, T., Brooks, J. C., Figueiredo, P., Wise, R., Matthews, P. M., & Tracey, I. (2005). Quantitative assessment of the reproducibility of functional activation measured with BOLD and MR perfusion imaging: Implications for clinical trial design. *NeuroImage*, 27, 393–401.
- Townsend, J. T., & Ashby, F. G. (1983). *Stochastic modeling of elementary psychological processes*. New York: Cambridge University Press.
- Twieg, D. B. (1983) The k-trajectory formulation of the NMR imaging process with applications in analysis and synthesis of imaging methods. *Medical Physics*, 10, 610–621.
- Uludag, K., & Buxton, R. B. (2004). Measuring the effects of indomethacin on changes in cerebral oxidative metabolism and cerebral blood flow during sensorimotor activation. *Magnetic Resonance in Medicine*, 51, 1088–1089; author reply 1090.
- Uludağ, K., Dubowitz, D. J., & Buxton, R. B. (2006). Basic principles of functional MRI. In R. R. Edelman, J. R. Hesselink, M. B. Zlatkin, & J. V. Crues III (Eds.), *Clinical magnetic resonance imaging* (3rd edn., Vol. 1, pp. 249–287). Philadelphia: Saunders Elsevier.

- Uludag, K., Dubowitz, D. J., Yoder, E. J., Restom, K., Liu, T. T., & Buxton, R. B. (2004). Coupling of cerebral blood flow and oxygen consumption during physiological activation and deactivation measured with fMRI. *NeuroImage*, 23, 148–155.
- Wang, J., Aguirre, G. K., Kimberg, D. Y., Roc, A. C., Li, L., & Detre, J. A. (2003). Arterial spin labeling perfusion fMRI with very low task frequency. *Magnetic Resonance in Medicine*, 49, 796–802.
- Wong, E. C., Buxton, R. B., & Frank, L. R. (1997). Implementation of quantitative perfusion imaging techniques for functional brain mapping using pulsed arterial spin labeling. *NMR in Biomedicine*, 10, 237–249.
- Wong, E. C., Buxton, R. B., & Frank, L. R. (1998a). Quantitative imaging of perfusion using a single subtraction (QUIPSS and QUIPSS II). *Magnetic Resonance in Medicine*, 39, 702–708.
- Wong, E. C., Buxton, R. B., & Frank, L. R. (1998b). A theoretical and experimental comparison of continuous and pulsed arterial spin labeling techniques for quantitative perfusion imaging. *Magnetic Resonance in Medicine*, 40, 348–355.
- Wong, E. C., Cronin, M., Wu, W. C., Inglis, B., Frank, L. R., & Liu, T. T. (2006). Velocity-selective arterial spin labeling. *Magnetic Resonance in Medicine*, 55, 1334–1341.
- Wong, E. C., Luh, W.-M., & Liu, T. T. (2000). Turbo ASL: Arterial spin labeling with higher SNR and temporal resolution. *Magnetic Resonance in Medicine*, 44, 511–515.
- Yang, S. P., & Krasny, J. A. (1995). Cerebral blood flow and metabolic responses to sustained hypercapnia in awake sheep. *Journal of Cerebral Blood Flow and Metabolism*, 15, 115–123.
- Zappe, A. C., Uludag, K., Rainer, G., & Logothetis, N. K. (2005). Influence of moderate hypercapnia on neural activity in monkey by simultaneous intracortical recordings and fMRI at 4.7T. In: 35th meeting, Society for Neuroscience, Washington D.C., p 10.11.
- Zarahn, E., Aguirre, G., & D'Esposito, M. (1997). A trial-based experimental design for fMRI. *Neuroimage*, 6, 122–138.